

IDŐJÁRÁS

Quarterly Journal of the Hungarian Meteorological Service
Vol. 126, No. 4, October – December, 2022, pp. 425–455

Impact of spatiotemporal land use and land cover changes on surface urban heat islands in a semiarid environment

Alireza Sadeghinia^{1,*} and Mahdi Sedaghat²

¹*Department of Geography Education*
Farhangian University, Tehran, Iran

²*Department of Geography*
Payame Noor University (PNU), Tehran, Iran

**Corresponding author E-mail: alirezasadeghinia@gmail.com*

(Manuscript received in final form August 30, 2021)

Abstract— This study presents the results of research that was conducted in the city of Tehran, located in the subtropics (35° N.) in a semi-desert climate in southwest Asia. The purpose was to analyze the relationship between land use/cover change (LULC) and the spatiotemporal dynamics of surface urban heat islands (SUHIs) and give results regarding the structure of the UHI in the city of Tehran. Using Landsat-5 TM data from 1986 to 2010, we quantified the spatiotemporal variability of the SUHI and LULC in the city of Tehran. The spatial distribution of land surface temperature (LST) showed the most extensive SUHI as spatially located in the western and southwestern areas of Tehran in 1986. In 2010, the spatial extent of SUHI had increased. The occurrence of LULC changes in the southern, southwestern, and especially the western parts of Tehran have played the most important role in expanding and intensifying the SUHI effect. These areas experienced two major alterations: (a) The area lost about 14 km² from green cover; and (b) the industrial and commercial land use, and transportation network extended significantly in these areas. Based on LULC and LST distribution patterns, barren lands, industrial and commercial land use, and transportation network have the major roles in the formation and expansion of the SUHI effect in Tehran. The SUHI of Tehran, like that of other arid or semi-arid cities, does not exhibit the classical pattern of SUHI: that is, the hot spots usually are not found in the downtown, as occurs in humid climates. Rather, the SUHI tends to situate over desert areas or barren lands that surround these cities. Therefore, an inversion of the standard SUHI phenomenon during daytime has been observed in Tehran. Research conducted in arid and semi-arid cities suggests that we should refine our point of view on the concept of the UHI in such cities and consider this issue in future studies.

Key-words: surface urban heat island, land use/cover change, land surface temperature, remote sensing, Tehran

1. Introduction

The urban heat island effect (UHI) is a critically important environmental disaster that has attracted researchers' attention for more than 150 years (*Streutker, 2003*). It refers to the phenomenon in which the air and surface temperature in an urban area is higher than that in its surrounding rural areas (*Yuan and Bauer, 2007*) and may be accompanied by a series of undesirable environmental effects such as adverse climate, urban diseases, and epidemics, worsened habitability, and greater energy demand for cooling. In other words, the UHI is the clearest expression of the effects of anthropogenic activity on climate at a local level (*Garcia-Cueto et al., 2007*).

Various methods applied to investigate the UHI effect in later decades generally comprised two approaches: conventional and remote sensing-based methods. The conventional techniques mostly have depended on mathematical and statistical methods (*Peterson, 2003; Arifwidodo and Tanaka, 2015*). Two types of indicators, air UHI (AUHI) and surface UHI (SUHI), have been widely used to study UHI (*Li et al., 2017*). The AUHI was calculated from the weather station network (*Chow and Roth, 2006; Karl and Quayle, 1988; Park et al., 2017*). The SUHI has been estimated from thermal infrared remote sensing techniques (*Dickinson et al., 2010; Li et al., 2017; Voogt and Oke, 2003; Zhou et al., 2014*). *Voogt and Oke (2003)* described in detail the use of thermal remote sensing in the study of urban climates, and believed that the thermal remote sensing techniques are suitable to study SUHI. First, SUHI were studied using NOAA AVHRR data (*Balling and Brazel, 1988; Dousset, 1989; Gallo et al., 1993; Gallo and Tarpley, 1996; Owen, 1998*); more recently, Landsat TM, ETM+, and ASTER data have been utilized for their higher spatial resolution (*Dai et al., 2010; Hamdi, 2010; Li et al., 2009, 2017; Liu and Zhang, 2011; Lu and Weng, 2006; Ranagalage et al., 2017; Sun et al., 2010; Weng, 2001, 2003; Weng et al., 2006, 2007; Weng and Lu, 2008; Xiao et al., 2008; Zhang et al., 2007*). Considering the close correspondence between the distribution of land surface temperature (LST) and land use and land cover (LULC) characteristics (*Weng and Lu, 2008*), numerous research articles have focused on exploring the relationship between LST and urban LULC change (*Amiri et al., 2009; Ifatimehin, 2011; Lazzarini et al., 2013; Lu and Weng, 2006; Pal and Ziaul, 2017; Weng, 2003, Weng and Lu, 2008; Zhou et al., 2014*). Understanding the relationships between LULC and LST can assist in urban planning for a better scientific understanding of how the encroachment of the urban land use can form and extend patterns of SUHI (*Weng, 2003*). Urban climate research has investigated the relationship with LST of factors such as vegetation abundance, soil moisture, and the roughness properties of the land surface (*Lo et al., 1997; Park et al., 2017; Soltani and Sharifi, 2017*). Meanwhile, the NDVI-LST relationships more than other indices have been examined (*Kim et al., 2005; Liu and Zhang, 2011; Ranagalage et al., 2017; Weng et al., 2004*). Recently, much attention has been paid to the NDBI-LST relationship in urban

areas. For example, *Liu and Zhang* (2011) showed that the negative correlation of LST and NDVI means that green land weakens the SUHI effect, whereas the positive correlation between LST and NDBI means that increased development strengthens it (*Liu and Zhang*, 2011). Most studies of changes in LST and LULC have emphasized that overdevelopment and degradation of vegetation cover have played an important role in strengthening and intensifying the SUHI effect (*Chen et al.*, 2006).

There is a need to utilize remote sensing data in investigating the LST of cities in dry and semi-dry environment; because these cities experience extremely high temperatures in warm seasons (*Rasul et al.*, 2017). The remote sensing techniques have been utilized to study some of the few SUHI studies in arid regions (*Amiri et al.*, 2009; *Balling and Brazil*, 1988; *Falahatkar*, 2011; *Garcia-Cueto et al.*, 2007; *Haashemi et al.*, 2016; *Lazzarini et al.*, 2013). The study of UHI, both atmospheric and surface, in the city of Mexicali showed a daily cycle in which the AUHI develops during the night but disappears in the daytime, giving way to an urban cold island. Comparing the LST of the urban area of Mexicali with its surrounding environs demonstrated that Mexicali does not show the classical pattern of AUHI; that is, higher surface temperatures are not only found closer to the urban center, as occurs in humid climates, but in this case, are also found in the surrounding desert areas.

The results of some UHI studies in arid regions were similar to those of Garcia-Cueto in the city of Mexicali (*Haashemi et al.*, 2016; *Lazzarini et al.*, 2013; *Zhou et al.*, 2015). *Lazzarini et al.* (2013) used remote sensing data from MODIS, ASTER, and LANDSAT7 to assess land cover–temperature interactions in the Abu Dhabi metropolitan area. Their results showed an inversion of the standard SUHI phenomenon in daytime, where the downtown areas appeared cooler than the suburbs with a daily difference of 5–6 °K in summer and 2–3 °K in winter. *Zhou et al.* (2015) examined the UHI effect in 32 major cities distributed throughout different climatic zones in China using MODIS, TM, ETM+ images during the period 2003–2012. They noted that the LST differences between urban and rural areas were significantly larger than those between urban and suburban areas during the day and night for the cities, except for Lanzhou and Tianjin in the daytime. In particular, Lanzhou demonstrated a cold island effect in comparison with surrounding rural areas.

Many scholars have explored UHI in the Tehran metropolitan area. In general, these studies had the following objectives: to study spatiotemporal variability of the UHI (*Bokaie et al.*, 2019; *Haashemi et al.*, 2016); to identify the possible causes of UHI in Tehran (*Shahmohamadi et al.*, 2015; *Shamsipour et al.*, 2012); to assess the relationship between LST and LULC (*Bokaie et al.*, 2016; *Rousta et al.*, 2018); to investigate the severity and impact of UHI on the environmental conditions of Tehran metropolitan area (*Shahmohamadi et al.*, 2013); and to explore the various models that could be implemented to mitigate the UHI effects in Tehran (*Shahmohamadi et al.*, 2013; *Sodoudi et al.*, 2014).

Despite these previous studies, the Tehran SUHI requires more research. Apparently, a more detailed assessment of the spatial patterns of UHI is needed to better understand the structure of the Tehran UHI. Our main objectives were (1) to explore the spatiotemporal variability of the Tehran SUHI between 1986 and 2010; (2) to analyze the spatial distribution of LST and its relationship with LULC; and (3) to analyze the structure of the Tehran SUHI as a semi-desert city.

2. Data and methodology

2.1. Study area

This research was conducted in a semi-desert area located in southwestern Asia, in the city of Tehran, the capital of Iran. Tehran (*Fig. 1*), with 8 million people, has the geographical coordinates of 35°33'10"N to 35°50'12"N and 51°05'17"E to 51°37'36"E with an average elevation of 1600 m and the high Alborz Mountains in its north and northeast. The Alborz Mountains partially reduce the area of dryness. The city has poor vegetation cover. In addition, the distribution of green spaces in the city is heterogeneous (*Haashemi et al., 2016*). This area is on the subtropical high pressure belt during the summer, which makes it warm and dry. Tehran has a cold semiarid climate (Köppen climate classification: BSK) with continental climate characteristics and a Mediterranean climate precipitation pattern. Tehran's climate can be generally described as mild in spring and autumn, hot and dry in summer, and cold and wet in winter. Most of the light annual precipitation occurs from late autumn to mid-spring, but no one month is particularly wet. The hottest month is July, and the coldest is January.

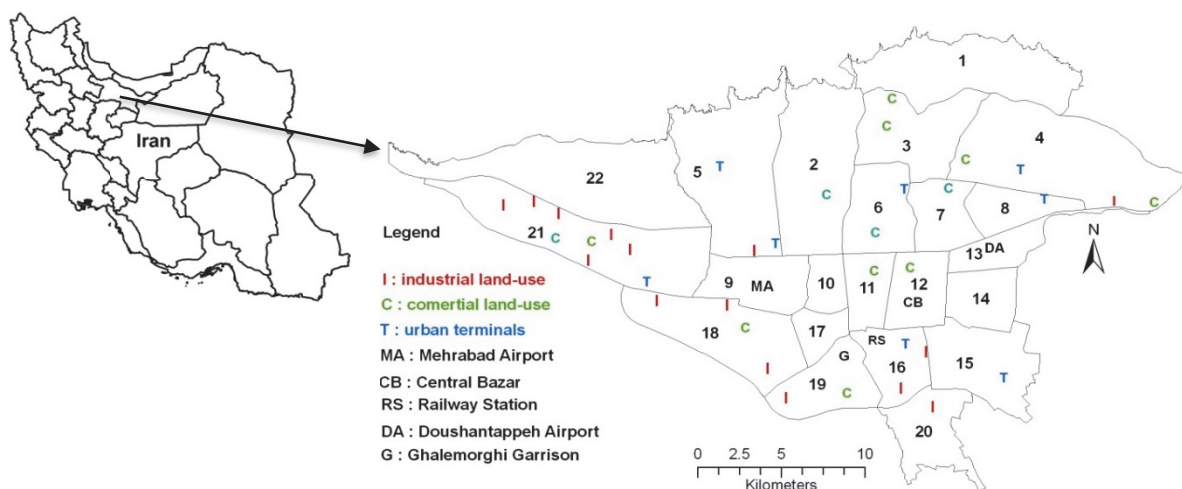


Fig 1. The study area. The most effective land use types for the establishment of UHI are presented on the map by their initials. The numbers represent the 22 districts of Tehran.

Tehran is divided into 22 municipal districts, each with its own administrative center. *Fig. 1* show the spatial distribution of 22 districts, industrial and commercial area, the central bazaar, the Mehrabad and Dooshantapeh airports, urban main terminals of railway stations, and other important phenomena that contribute to the formation of hot spots in the Tehran metropolitan area. Tehran is the most important center of population, culture, industry, commerce, and transportation in Iran, encroaching on the limited surrounding agricultural areas (*Malekpour et al.*, 2010). Because of its complicated expansion, structure, and function, temperature variations are very important for its life and existence. Thus, this study has tried to analyze the relationship between the spatiotemporal distribution of SUHI and LULC change in Tehran.

2.2. Data and image preprocessing

Change detection can be defined as the process of identifying differences in the state of an object or phenomenon by observing it at different times. Using multi-sensor images to change detection is a challenge in terms of designing a suitable procedure. Ideally, change detection is conducted with multi-temporal images from the same sensor (*Lu et al.*, 2014). In this paper, two landsat-5 TM images acquired on June 2, 1986 and June 4, 2010 were used to extract LST and LULC information. Some assistant data such as the air temperature and the air moisture were collected from five weather stations on June 2, 1986 and June 4, 2010 used as the input parameters to retrieve LST. The data preprocessing and other analyses were performed using ERDAS Imagine 9.2 and ArcGIS 9.3 software.

2.3. Derivation of LST

Two Landsat-5 TM images acquired on June 2, 1986 and June 4, 2010, respectively, were used to extract LST and LULC information. Some auxiliary data such as the air temperature and air moisture were collected from five weather stations on June 2, 1986 and June 4, 2010 used as the input parameters to retrieve LST. Data preprocessing and other analyses were performed using ERDAS Imagine 9.2 and ArcGIS 9.3 software.

A mono-window algorithm was applied to obtain LST from the thermal band (band 6) of Landsat TM images (*Qin et al.*, 2001):

$$T_s = \{a(1 - C - D)[b(1 - C - D) + C + D]T_i - DT_a\}/C \quad (1)$$

With $C = \varepsilon_i \times \tau_i$, $= (1 - \tau_i)[1 + (\varepsilon_i) \times \tau_i]$, $a = -67.355351$ and $b=0.458606$, where ε_i is emissivity, τ_i is the total atmospheric transmittance, T_i is the at-sensor brightness temperature (in K), and T_a represents the effective mean atmospheric temperature given by

$$T_a = 16.0110 + 0.92621 \times T_o \quad (2)$$

where T_o is the near surface temperature.

Qin et al. (2001) estimated the atmospheric transmittance from the atmospheric water vapor content (w) according to *Table 1*. Both T_o and w were obtained from local meteorological stations.

Table 1. Estimation of atmospheric transmittance (*Qin et al.*, 2001)

Profiles equation (τ_i)	water vapor (w) (g/cm ²)	Transmittance estimation
High air temperature	0.4 - 1.6	0.974290 – 0.08007 w
	1.6 - 3.0	1.031412 – 0.11536 w
Low air temperature	0.4 - 1.6	0.982007 - 0.09611 w
	1.6 - 3.0	1.053710 - 0.14142 w

The emissivity can be estimated using the Normalized Difference Vegetation Index, *NDVI* (*Van De Griend and Owe*, 2003). A complete land surface emissivity estimation method proposed by *Zhang et al.* (2006) was utilized to calculate emissivity for each pixel (*Table 2*).

Table 2. Estimation of emissivity by using *NDVI* (*Zhang et al.*, 2006)

<i>NDVI</i>	Land surface emissivity (ϵ_i)
$NDVI < -0.185$	0.995
$-0.185 \leq NDVI \leq 0.157$	0.97
$0.157 \leq NDVI \leq 0.727$	$1.0094 + 0.047 \ln (NDVI)$
$NDVI > 0.727$	0.99

2.4. Detection of LST spatiotemporal dynamics

To examine the spatial distribution of LST data during the study period and reduce the influence of seasonal difference, the resultant LST images are divided into three levels, high- (L3), normal- (L2), and low-temperature (L1) ranges (three levels), using a robust statistical method proposed by *Zhang et al.* (2007). The proposed method can be applied when the LST images follow a normal distribution. Based on *Fig. 2*, the histogram distribution of LST images for both

1986 and 2010 follow a normal distribution. In this method, the average temperature(u) ± 1 standard deviation (std) is set as two threshold values that divide the LST into three ranges. *Table 3* shows the temperature classification method. The area with LST above $u+std$ would be defined as a heat island; by contrast, the area with LST below $u-std$ would be defined as a cold island. The annual difference between the mean surface temperature of the heat and cold islands could be propounded as the SUHI intensity in the study area.

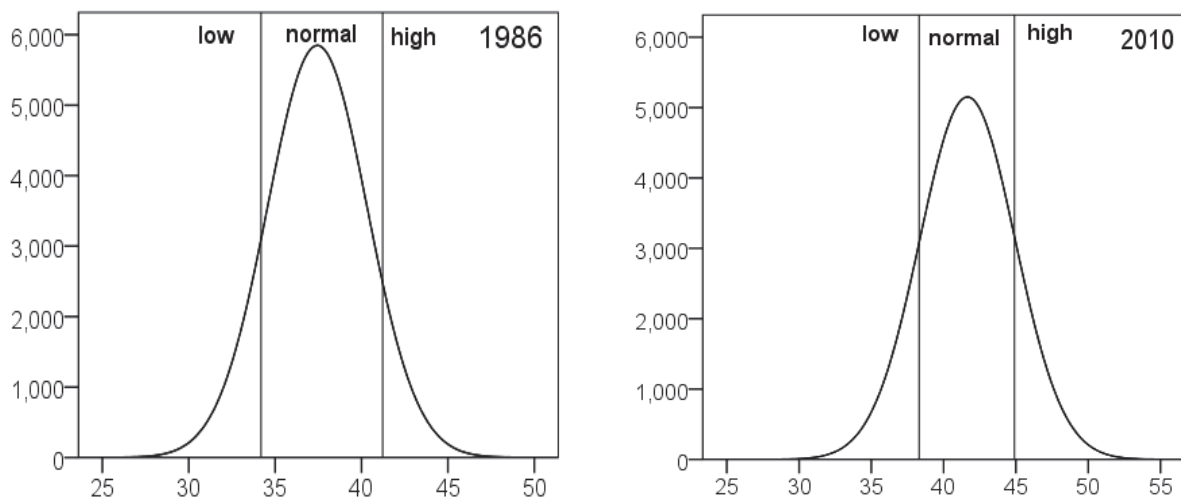


Fig 2. Distribution of LST (C°) for June 2, 1986 and June 4, 2010.

Table 3. Temperature ranges for classification of LST images

temperature classification	interval of temperature classification
high temperature area (L ₃)	$LST > u + std$
normal temperature area (L ₂)	$u - std < LST < u + std$
low temperature area (L ₁)	$LST < u - std$

2.5. LULC classification

The proposed method by *Xu (2007)* was used to classify the LULC types in the study area. Based on the previous studies, the urban ecosystem can be broken down into several components, including impervious surface material, green

vegetation, exposed soil, and water (*Chen et al.*, 2006; *Xu*, 2007). Accordingly, the urban area can reasonably be classified into four generalized categories (i.e., built-up land, green cover, bare land, and water). In this study, to characterize these categories, the Normalized Difference Built-up Index (*NDBI*), Soil Adjusted Vegetation Index (*SAVI*), Normalized Difference Bareness Index (*NDBaI*) and Modified Normalized Difference Water Index (*MNDWI*) were applied. *MNDWI* can be employed to detect water features in an urban area. *Xu* (2007) showed that *MNDWI* can enhance the contrast between water and other land use (built-up, bare land and green cover) because other categories reflect *MIR* (*TM5*) radiation much higher than *NIR* (*TM2*) radiation. In the *MNDWI* image, the built-up land, bare land, and green land have negative values, but the water has a positive value. Therefore, *MNDWI* helps distinguish the water class from the others. *MNDWI* is expressed as follows (*Xu*, 2005):

$$MNDWI = \frac{Green - MIR}{Green + MIR} \quad (3)$$

Then, a simple logic statement can easily extract the water pixels from other land uses. According to the spatial model maker tools in ERDAS 9.1, the function is as follows:

EITHER 1 IF (MNDWI>0) OR 0 OTHERWISE.

Although *NDVI* is the most important vegetation index, in this study the *SAVI* index was employed to highlight vegetation features because *SAVI* is more suitable in an area with low plant cover such as urban areas (*Ray*, 1994; *Xu*, 2007). *SAVI* can work in areas with plant cover as low as 15%, whereas *NDVI* can only work effectively in areas with plant cover above 30% (*Ray*, 1994). The *SAVI* can be calculated using the following equation (*Huete*, 1988):

$$SAVI = \frac{(NIR - Red)(1 + I)}{NIR + Red + I} \quad (4)$$

Where *I* is a correction factor that ranges from 0 for very high densities to 1 for very low densities. Given an intermediate vegetation density in the study area, a value of 0.5 was used. As for water, a simple logic statement could be used to extract vegetation pixels from others:

EITHER 1 IF (SAVI>0) OR 0 OTHERWISE.

Our studies showed numberless mixed pixels mostly comprising vegetation in combination with bare or built-up land. To prevent noise, these pixels were extracted through determination of a suitable threshold for *SAVI*. The logic calculation can be expressed as follows:

EITHER 1 IF ($SAVI > -0.1$ and $SAVI < 0$) OR 0 OTHERWISE.

Another index, *NDBI*, is sensitive to the built-up area (*Zha et al.*, 2003). The *NDBI* image is calculated by the following equation:

$$NDBI = \frac{MIR - NIR}{MIR + NIR}. \quad (5)$$

NDBI is a suitable index for extracting the built-up land from urban areas (*Liu and Zhang*, 2011), because the built-up lands have higher reflectance in *MIR* than *NIR* (*Xu*, 2007). However, *Gao* (1996) and *Xu* (2007) showed that in some circumstances, drier vegetation and water with high suspended matter concentration can also reflect *MIR* more strongly than *NIR* and, as a result, they will have positive *NDBI* values and present as noise in an *NDBI* image. Additionally, *Chen et al.* (2006) also found that *NDBI* is not sufficient to differentiate the bare land from the built-up area, because both have relatively similar spectral characteristics. Consequently, the contrast of the *NDBI* image is not as good as *SAVI* and *MNDWI* images, because many pixels of vegetation, water and bare land to be mixed with built-up area.

The last index used in this study is *NDBaI*, proposed by *Zhao and Chen* (2005) to retrieve bare land from the Landsat imagery. *NDBaI* can be calculated for Landsat imagery using the following equation:

$$NDBaI = \frac{\text{band 5} - \text{band 6}}{\text{band 5} + \text{band 6}}. \quad (6)$$

In Landsat imagery, the spectral characteristic of band 5 – band 6 > 0 is highly consistent with bare land, so bare land can be distinguished approximately using images with $NDBaI > 0$. However, the proposed threshold ($NDBaI > 0$) is not constant; it will change little in different regions or in different conditions of atmosphere and precipitation (*Chen et al.*, 2006). Despite *NDBaI*'s relative efficiency, it is not enough to differentiate the bare land from the built-up area. Based on the explanations mentioned, urban built-up and bare land could not be extracted merely based on *NDBI* and *NDBaI* images. Therefore, this study combines the *NDBI*, *NDBaI*, *SAVI*, and *MNDWI* to extract built-up and bare land area. Based on the previous studies (*Xu*, 2007), this method can improve classification accuracy.

To achieve this object, first the *SAVI*, *MNDWI*, *NDBI*, and *NDBaI* images were produced, and then a new four band image was created through a layered stack of four images. Two methods were used to extract built-up and bare land from the new images (the new four-band image): principal component analysis (*PCA*) and logic calculation. First, *PCA* was performed on the two new images (June 2, 1986 and June 4, 2010). *Table 4* shows the results of the *PC* transformation on the new images based on the covariance matrix. The values in

the table provide the basis for determining which *PC* has the greatest loadings (values) for *NDBI* or *NDBaI* bands (representing the built-up and bare land classes), and there is also a considerable difference between loadings of bands. It is obvious that in *PC1* and *PC2*, *MNDWI* and *SAVI* have the greatest loadings, respectively; consequently, built-up and bare land cannot be identified from *PC1* and *PC2*. In *PC4*, although the *NDBI* band has a big loading (0.81, 0.83), the *SAVI* and *MNDWI* bands also have positive loadings in the two image and are difficult to separate from one another. Our exploration also confirmed that *PC4* is not suitable for extracting built-up and bare land. Therefore, *PC3* is more suitable than the others for separating built-up and bare land because the *NDBaI* band has a strong positive loading and the *NDBI* band has a small positive loading, in addition to the *MNDWI* band, which has a strong negative loading in *PC3* that entirely helps to differentiate LULC types. Spectral signature analysis represented by the mean of urban land use for 1986/6/2 also confirmed that *PC3* is more efficient than *PC4* for extracting both built-up and bare land, because built-up features have negative values, whereas bare lands have negative values in *PC3* (see Fig. 3). Finally, the suitable threshold values were used to extract built-up and bare land from the *PC3* image. According to the spatial model maker tools in ERDAS 9.1 software, the conditional function is as follows:

$$\text{CONDITIONAL } \{(PC3 < 0) <1>, (PC3 \geq 0) <2>\},$$

where <1> and <2> are built-up and bare land respectively.

To evaluate classification accuracy, a random sampling method was used, with a total of 150 pixels sampled for each image. Then, the accuracy of the classification maps was verified by field study or by comparing with existing LULC maps. The overall accuracy was 89.1% for 1986 and 90.7% for 2010. The Kappa coefficient was 0.87 and 0.89 for 1986 and 2010, respectively. The precision of the classification results show that they are good enough for further spatiotemporal analysis.

Table 4. Principal component analysis on the two new four-band images

		June 2, 1986 image				June 4 2010 image			
		<i>PC1</i>	<i>PC2</i>	<i>PC3</i>	<i>PC4</i>	<i>PC1</i>	<i>PC2</i>	<i>PC3</i>	<i>PC4</i>
Eigenvectors	<i>SAVI</i> -band	0.47	0.67	0.35	0.45	0.49	0.7	0.27	0.41
	<i>NDBI</i> -band	-0.5	-0.25	0.13	0.81	-0.42	-0.27	0.21	0.83
	<i>NDBaI</i> -band	0.31	-0.55	0.76	-0.10	0.41	-0.49	0.74	-0.14
	<i>MNDWI</i> -band	0.64	-0.41	-0.52	0.35	0.64	-0.41	-0.56	0.32

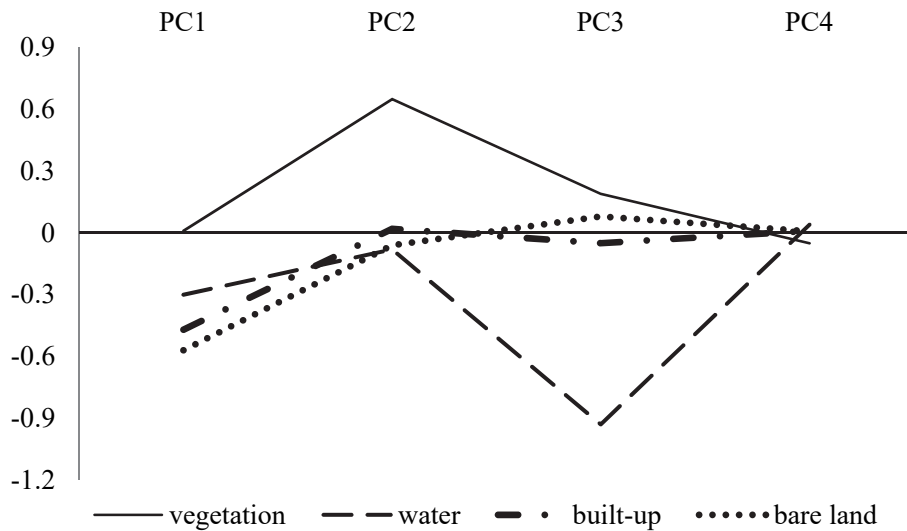


Fig 3. Spectral signatures represented by the mean of urban land use classes of Tehran for June 2, 1986 as an example.

3. Results

3.1. Spatiotemporal distribution of SUHI

Fig. 4 represents the general pattern of LST spatial distribution in Tehran for both 1986 and 2010. In these maps, the LST data were classified into three groups based on the classification scheme of standard deviation that aforesaid in methodology section. The LST patterns show significant differences between the western and southwestern parts of Tehran in comparison with the northern part. The statistics of LST of each image are summarized in Table 5.

Table 5. Summary statistics of LST data for Tehran (°C)

Date of image	mean	maximum	minimum	Standard deviation	SUHI intensity
June 2, 1986	37.2	47	11	3.02	10
June 4, 2010	41.6	54	27	3.3	10.15

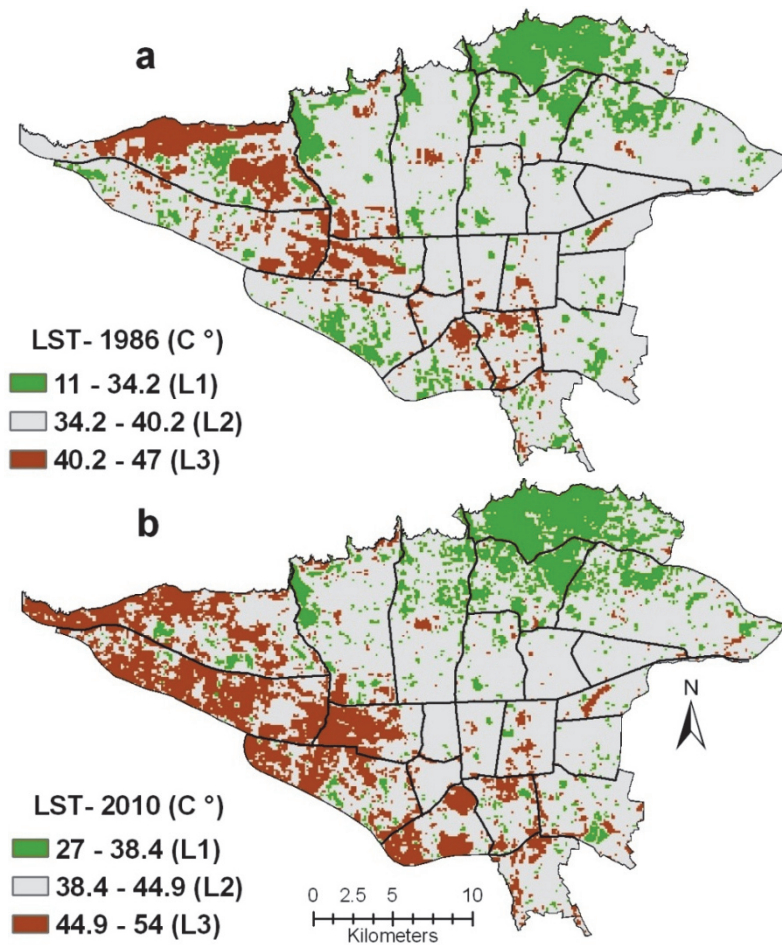


Fig 4. LST distribution images in June 2, 1986 (a) and June 4, 2010 (b).

The statistics of LST on June 2, 1986 indicates that the lowest LST was 11 °C, the highest LST was 47 °C, and the mean was 37.2 °C, with a standard deviation of 3.02. In 1986, some hot spots can be clearly observed (*Fig 5a*). The most extensive hot spots were distributed in the western and southwestern parts of Tehran, over Mehrabad international airport, its surrounding barren land, and a special industrial zone in the west of Tehran. The hottest part of the Tehran SUHI is located over the Mehrabad international airport with approximate area of 900 hectares in district 9. The other hot spots are dispersed all over the city, especially in the old downtown and central bazaar, Dooshantappeh airport, the railway station, bus terminals, grain silo, and factories (see *Fig. 1* for their spatial positions). However, the coldest area of Tehran (cold island) was located in the green land area north of Tehran, especially in the Shemiranat and considerable portions of districts 2, 3 and 4. The other dispersed cold spots mostly correspond to green areas and urban parks, with the parks being the coolest spots. The spatial

pattern of LST on June 4, 2010 differs markedly from that of June 2, 1986, as *Fig. 4* shows. The statistics of LST on June 4, 2010 indicates that the lowest LST was 27 °C, the highest LST was 54 °C, and the mean was 41.6 °C, with a standard deviation of 3.3 (*Table 5*). The most significant difference between 1986 and 2010 is seen in the western, southwestern, and southern parts of Tehran. Although the most extensive SUHI, previously located in the western and southwestern area of the study area, has slightly shifted to the westward in 2010, its extent has increased. Two major hot spots appeared in the south of district 19 (the southern part of Tehran), and a major hot spot was formed in the southwestern part of the city over district 18. Several hot spots also appeared in the western area over districts 21 and 22.

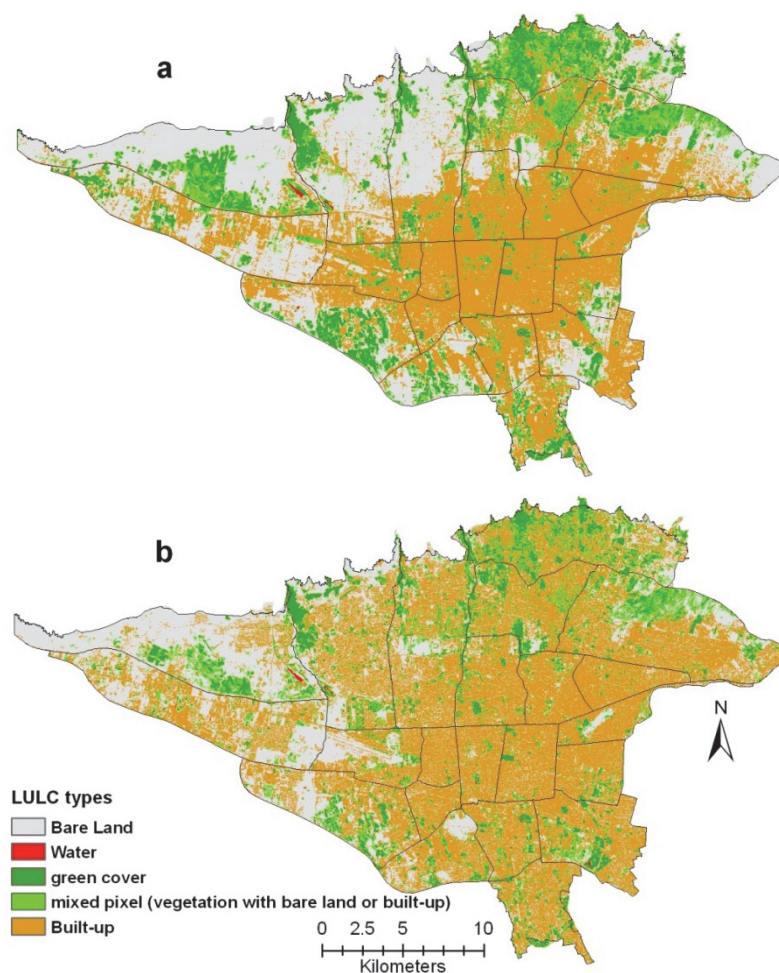


Fig. 5. the LULC distribution in June 2, 1986 (a) and June 4, 2021 (b)

Based on the distribution pattern of hot spots in the period 1986–2010 that characterized the Tehran SUHI, it does not exhibit the classical SUHI pattern like

that of other cities that have been located in arid or semiarid climates; that is, the hot spots usually are not found in central parts of cities, as occurs in humid climates, but instead they tend to situate over desert areas and surrounding bare lands. Therefore, an inversion of the standard SUHI phenomenon has been observed during daytime in Tehran, where the downtown area appears colder than the western, southwestern, and southern areas. This finding confirms the results of Haashemi *et al.* (2016) regarding the structure of the Tehran SUHI.

The result described above has also been observed in other arid and semi-arid cities such as Phoenix (Balling and Brazil, 1988), Mexicali (Garcia-Cueto *et al.*, 2007), and Abu Dhabi (Lazzarini *et al.*, 2013).

The results of three temperature areas and the associated changes in each class from 1986 to 2010 are listed in *Table 6*. Class 1 (L₁) comprises values with more than one standard deviation below the mean that shows cold islands; class 2 (L₂) values are normal values situated between the mean and one standard deviation below or above the mean; and class 3 (L₃) values are heat islands with more than one standard deviation above the mean. According to the resulting table, the high-temperature area (L₃) has increased about 31 km² from 1986 to 2010; in contrast, the low-temperature area has decreased about 3 km². The values in *Table 3* also show that SUHI intensity has increased slightly over time, from 10 °C in 1986 to 10.2 °C in 2010. Furthermore, based on the evolution process of LST data pattern from 1986 to 2010, the area and intensity of the Tehran SUHI has rapidly spread and strengthened, while the cold urban island has weakened.

Table 6. Area in different temperature scales from 1986 to 2010 (km²)

Range	Area in 1986	Area in 2010	Change between 1986 to 2010
High temperature area (L3)	83	114	+31
Normal temperature area (L2)	449	421	-28
Low temperature area (L1)	82	79	-3

3.2. Relationship between LULC characteristics and SUHI patterns

Table 7 summarizes the average LST value of LULC types. The highest and lowest surface temperature relate to bare lands and water bodies, respectively. After bare lands, which exhibited the highest surface temperature in the study area (38.3 °C in 1986 and 43.3 in 2010), built-up areas had the highest surface temperature (37.8 °C in 1986 and 41.5 °C in 2010), followed by mixed pixels (35.4 °C in 1986 and 39.8 °C in 2010), green cover (32.9 °C in 1986 and 37.6 °C in 2010), and water bodies (30.3 °C in 1986 and 33.2 °C in 2010). The maximum LST difference of LULC types was 8 °C and 10 °C in 1986 and 2010, respectively.

Therefore, the difference between the average value of surface temperature of water bodies (the coldest of land cover) and bare lands (the hottest land cover) has increased about 2 °C. The average values of LULC types for both 1986 and 2010 implies that bare lands and built-up areas have played the major roles in forming and expanding SUHI effects in Tehran. Of course, all the built-up areas did not exhibit the same surface temperature; some land use, such as transport and industrial land use, displayed higher surface temperatures than residential land use. Apparently, residential land use is less effective in promoting hot spots in Tehran. Spatially, the Tehran SUHI has been closely related to bare lands and to transport and industrial land use. These areas mostly have been covered with non-evaporating, non-transpiring materials such as asphalt, metal, concrete, and stone. In contrast, green lands showed considerably lower LST, because vegetation can reduce the amount of stored heat in the land surface through evapotranspiration and shadow. Extensive green spaces in the northern part of Tehran (districts 1, 2, 3, and 4) contributed to lower surface temperatures and the formation of an urban cold island there.

Table 7. The mean value of LST of LULC types

LULC types	Mean temperature (1986)	Mean temperature (2010)
Water	30.3	33.2
Green cover	32.9	37.6
Mixed pixel	35.4	39.8
Built-up	37.8	41.5
Bare land	38.3	43.3

Fig. 5 shows LULC distribution in Tehran for 1986 and 2010. The built-up areas dominated in both 1986 and 2010, occupying about 247.2 km² (40%) and 310.7 km² (50%), respectively (Table 8). Although the built-up area has increased about 64 km² from 1986 to 2010, areas of other LULC have decreased. Water bodies can be disregarded, because they have very small surface area. Because built-up areas have expanded in all directions, the bare lands and green lands lost about 37.5 km² and 23.9 km², respectively. LULC changes in the southern, southwestern, and particularly the western parts have played an important role in expanding and intensifying the SUHI effect in our study area. Because of the expansion of industrial and commercial land use and the development of the transportation network in the western and southwestern parts, several hot spots (or urban heat islands) have appeared. The most expansion of the industrial land use has occurred along the western highways, such as the Karaj highway and the old Karaj road. Similar changes have also occurred in district 18 (southwest of Tehran) and 19 (the south of Tehran). The other important alteration has occurred

in the vegetation cover areas of districts 18, 19, 20, 21, and 22 (the west, south, and southwest of Tehran). Based on our analysis, these districts lost vegetation cover of about 4.6, 1.3, 2.0, 2.8, and 3.3 km² respectively. The largest LST pattern alteration occurred in areas in which dark (asphalt, tar, concrete, etc.) and metallic materials (galvanized or aluminum roofs) replaced the concentrated vegetation cover. The industrial and commercial land use areas, transportation network, and warehouses are mostly covered by dark materials and metallic roofs; consequently, they are associated with a high LST. In the bare lands and desert areas, because of the dry nature of non-evaporating materials, the LST is high.

Table 8. Area of LULC types in Tehran from 1986 to 2010

LULC types	Area (1986) km ²	Area (2010) km ²	Change in LULC between 1986 to 2010
Water	0.35	0.34	-0.1
Green cover	76.6	52.7	-23.9
Mixed pixel	49.8	47.6	-2.2
Built-up	247.2	310.7	63.5
Bare land	237	199.5	-37.5

4. Conclusion

In this study, the relationship between LULC changes and the spatiotemporal dynamics of the SUHI of Tehran, Iran were investigated for 1986 and 2010. The results showed that the area of SUHI has increased about 31 km², whereas the urban cold island (UCI) area has decreased about 3 km². The SUHI intensity (SUHII) also slightly increased. The most extensive SUHI was spatially located in the western and southwestern parts of Tehran in 1986. However, in 2010, SUHI has slightly shifted westward, and its extent has increased; new hot spots have appeared in the western, southwestern and southern parts of Tehran. The highest LST relates to bare lands and built-up areas, followed by mixed pixels, green cover, and water bodies. The precise consideration of LST in the study area indicates that bare lands, industrial and commercial land use areas, and the transportation network have played major roles in the formation and expansion of the SUHI effect in Tehran; in contrast, the residential land use area is less effective in promoting the SUHI effects. In the period 1986–2010, the built-up area increased about 64 km², but the bare lands and green lands lost about 37.5 km² and 23.9 km², respectively. The occurrence of LULC changes in the southern,

southwestern, and especially the western areas of Tehran have played the most important role in expanding and intensifying the SUHI effect. These areas experienced two major alterations: (a) districts 18, 19, 20, 21, and 22 lost about 14 km² from green vegetation cover from 1986 to 2010; (b) the industrial and commercial land use areas and the transportation network increased extensively in these areas. This study showed that in arid and semiarid cities, the largest alteration of LST occurs in areas where dark (asphalt, tar, concrete, etc.) and metallic materials (galvanized or aluminum roofs) replace the concentrated vegetation cover (similar to those changes in the western and southwestern areas of Tehran). Therefore, protection and expansion of vegetation cover has great importance in mitigating the SUHI effect. It seems that in semi-desert cities such as Tehran, where dry bare lands, industrial and commercial land use areas, and extensive transportation networks situated together on the city outskirts provide an opportunity for the emergence of an extensive SUHI.

The spatial distribution pattern of the SUHI phenomenon in our study area indicated that the SUHI of arid and semiarid cities (such as Tehran) differ considerably from that of cities situated in humid climates, which usually exhibit the classical SUHI pattern. In other words, the SUHI is usually located downtown, but in arid and semiarid cities, the SUHI tends to be situated over desert areas or extensive bare lands located in the suburbs. Based on the spatial distribution of the LST in Tehran, the highest LST is not observed over the downtown area, but rather increases as we move from the downtown toward the west, southwest, south, and east. The change pattern from the downtown toward the north area differs from that in other directions. Toward the northern area (districts 1, 2, 3, and 4), the LST decreases away from the downtown, because the maximum vegetation rate is concentrated in the northern area of the city. Therefore, an inversion of the standard daytime SUHI phenomenon has been observed in Tehran. Our results regarding the structure of SUHI in Tehran correspond to the results of other research exploring the UHI in dry and semiarid cities (*Balling and Brazil, 1988; Garcia-Cueto et al., 2007; Haashemi et al., 2016; Lazzarini et al., 2013*). For instance, *Garcia-Cueto et al., (2007)* examined AUHI and SUHI and their relationship with LULC in the city of Mexicali. Their results showed that during the daytime, in any season of the year, the city becomes a UCI. They found that Mexicali does not show the classical pattern of a UHI; that is, the higher surface temperatures are not only found toward the downtown, as occurs in humid climates (*Garcia-Cueto et al., 2007*). Also, the study of the Abu Dhabi SUHI showed a daytime inversion of the standard SUHI phenomenon in which the downtown areas appeared colder than the suburbs. Abu Dhabi has a hot desert climate (*Lazzarini et al., 2013*). *Zhou et al., (2015)* investigated the UHI in 32 Chinese cities. Their results showed that the direction of the UHI might be reversed in cities such as Lanzhou located in an arid climate. Lanzhou presented the cold island effect (negative) in comparison with rural areas (*Zhou et al., 2015*). Our results resembled the findings of *Haashemi et al., (2016)*, suggesting that, in

semiarid cities such as Tehran, with the urban–rural indicator, a surface urban cool island may be observed in daytime. Therefore, research conducted in arid and semiarid cities suggests the need to refine our point of view on the concept of UHI in arid and semiarid cities and consider this issue in future studies.

References

- Amiri, K., Weng, Q., Alimohamadi, A., and Alavipanah, K., 2009: Spatial–temporal dynamics of land surface temperature in relation to fractional vegetation cover and land use/cover in the Tabriz urban area, Iran. *Remote Sens. Environ.* 113, 2606–2617. <https://doi.org/10.1016/j.rse.2009.07.021>
- Arifwidodo, S.D. and Tanaka, T., 2015: The Characteristics of Urban Heat Island in Bangkok, Thailand. *Procedia – Soc. Behavior. Scie.* 195, 423–428. <https://doi.org/10.1016/j.sbspro.2015.06.484>
- Balling, R.C. and Brazell, S.W., 1988: High resolution surface temperature patterns in a complex urban terrain. *Photogram. Engineer. Remote Sens.* 54, 1289–1293.
- Bokaie, M., Zarkesh, M.K., Arasteh, P.D., and Hosseini, A., 2016: Assessment of urban heat island based on the relationship between land surface temperature and land use/land cover in Tehran. *Sustain. Cities Soc.* 23, 94–104. <https://doi.org/10.1016/j.scs.2016.03.009>
- Bokaie, M., Shamsipour, A., Khatibi, P., and Hosseini, A., 2019: Seasonal monitoring of urban heat island using multi-temporal Landsat and MODIS images in Tehran. *Int. J. Urban Sci.* 23, 269–285. <https://doi.org/10.1080/12265934.2018.1548942>
- Chen, X.L., Zhao, H.M., Li, P.X., and Yin, Z.Y., 2006: Remote sensing image-based analysis of the relationship between urban heat island and land use/cover changes. *Remote Sens. Environ.* 104, 133–146. <https://doi.org/10.1016/j.rse.2005.11.016>
- Chow, W.T.L. and Roth, M., 2006: Temporal dynamics of the urban heat island of Singapore. *Int. J. Climatol.* 26, 2243–2260. <https://doi.org/10.1002/joc.1364>
- Dai, X., Guo, Z., Zhang, L., and Li, D., 2010: Spatio-temporal exploratory analysis of urban surface temperature field in Shanghai, China. *Stoch. Environ. Res Risk Assess.* 24, 247–257. <https://doi.org/10.1007/s00477-009-0314-2>
- Dickinson, J.L., Zuckerberg, B.J., and Bonter, D.N., 2010: Citizen science as an ecological research tool: challenges and benefits. *Ann. Rev. Ecol. Evol. Syst.* 41, 149–172. <https://doi.org/10.1146/annurev-ecolsys-102209-144636>
- Dousset, B., 1989: AVHRR-derived cloudiness and surface temperature patterns over the Los Angeles area and their relationship to land use. Proceedings of IGARSS-89. New York, NY: IEEE, 2132–2137.
- Falahatkar, S., Hosseini, S.M., and Soffianian, A.R., 2011: The relationship between land cover changes and spatial-temporal dynamics of land surface temperature. *Indian J. Sci. Technol.* 4(2), 76–81. <https://doi.org/10.17485/ijst/2011/v4i2/29937>
- Gallo, K.P., McNab, A.L., Karl, T.R., Brown, J.F., Hood, J.J., and Tarpley, J.D., 1993: The use of NOAA AVHRR data for assessment of the urban heat island effect. *J. App. Meteorol.* 32, 899–908. [https://doi.org/10.1175/1520-0450\(1993\)032<0899:TUONAD>2.0.CO;2](https://doi.org/10.1175/1520-0450(1993)032<0899:TUONAD>2.0.CO;2)
- Gallo, K.P. and Tarpley, J.D., 1996: The comparison of vegetation index and surface temperature composites for urban heat island analysis. *Int. J. Remote Sens.* 17, 3071–3076. <https://doi.org/10.1080/01431169608949128>
- Gao, B.C., 1996: NDWI—A normalized difference water index for remote sensing of vegetation liquid water from space. *Remote Sens. Environ.* 58, 257–266. [https://doi.org/10.1016/S0034-4257\(96\)00067-3](https://doi.org/10.1016/S0034-4257(96)00067-3)
- Garcia-Cueto, Jauregui-Ostos, E., and Tejada-Martinez, A., 2007: Detection of the urban heat island in Mexicali, B.C., Mexico and its relationship with land use. *Atmosfera*, 20(2), 111–131.
- Haashemi, S., Weng, Q., Darvishi, A., and Alavipanah, S.K., 2016: Seasonal Variations of the Surface Urban Heat Island in a Semi-Arid City. *Remote Sens.* 8, 352. <https://doi.org/10.3390/rs8040352>

- Hamdi, R., 2010: Estimating Urban Heat Island Effects on the Temperature Series of Uccle (Brussels, Belgium) Using Remote Sensing Data and a Land Surface Scheme. *Remote Sens.* 2, 2773–2784. <https://doi.org/10.3390/rs2122773>
- Huete, A.R., 1988: A soil-adjusted vegetation index (SAVI). *Remote Sens. Environ.* 25(3), 295–309. [https://doi.org/10.1016/0034-4257\(88\)90106-X](https://doi.org/10.1016/0034-4257(88)90106-X)
- Ifatimehin, O., Musa, S.D. and Adeyemi, J.O., 2011: Managing Land use transformation and land surface temperature change in Anygiba town, Kogi state, Nigeria. *J. Geograp. Geol.* 3, 77–85. <https://doi.org/10.5539/jgg.v3n1p77>
- Karl, T.R. and Quayle, R.G., 1988: Climate change in fact and in theory: Are we collecting the facts? *Climate Change*, 13, 5–17. <https://doi.org/10.1007/BF00140159>
- Kim, H.M., Kim, B.K., and You, K.S., 2005: A statistic correlation analysis algorithm between land surface temperature and vegetation index. *Int. J. Inform. Proc. Syst.* 1, 102–106. <https://doi.org/10.23953/cloud.ijaese.204>
- Lazzarini, M., Marpu, P.R., and Ghedira, H., 2013: Temperature-land cover interactions: The inversion of urban heat island phenomenon in desert city areas. *Remote Sens. Environ.* 130, 136–152. <https://doi.org/10.1016/j.rse.2012.11.007>
- Li, J.J., Wang, X.R., Wang, X.J., Ma, W.C., and Zhang, H., 2009: Remote sensing evaluation of urban heat island and its spatial pattern of the Shanghai metropolitan area, China. *Ecol. Complex.* 6, 413–420. <https://doi.org/10.1016/j.ecocom.2009.02.002>
- Li, W., Coa, Q., Lang, K., and Wu, J., 2017: Linking potential heat source and sink to urban heat island: Heterogeneous effects of landscape pattern on land surface temperature. *Sci. Total Environ.* 586, 457–465. <https://doi.org/10.1016/j.scitotenv.2017.01.191>
- Liu, L. and Zhang, Y., 2011: Urban heat island analysis using the Landsat TM data and ASTER data: a case study in Hong Kong. *Remote Sens.* 3, 1535–1552. <https://doi.org/10.3390/rs3071535>
- Lo, C.P., Quattrochi, D.A., and Luvall, J.C., 1997: Application of high-resolution thermal infrared remote sensing and GIS to assess the urban heat island effect. *Int. J. Remote Sens.* 18, 287–304. <https://doi.org/10.1080/014311697219079>
- Lu, D. Li, G., and Moran, E., 2014: Current situation and needs of change detection techniques. *Int. J. Image Data Fusion* 5, 13–38. <http://dx.doi.org/10.1080/19479832.2013.868372>
- Lu, D. and Weng, Q., 2006: Spectral mixture analysis of ASTER imagery for examining the relationship between thermal features and biophysical descriptors in Indianapolis, Indiana. *Remote Sens. Environ.* 104, 157–167. <https://doi.org/10.1016/j.rse.2005.11.015>
- Malekpour, P., Taleai, M., and Rezaei, Y., 2010: Remote sensing-based spatial-temporal analysis of urban land surface temperature related to urban development: a case study of Tehran, MRSS2010, 6th International Remote Sensing and GIS Conference and Exhibition, April 28–29, 2010, Putra World Trade Centre, Kuala Lumpur, Malaysia.
- Owen, T.W., Carlson, T.N., and Gillies, R.R., 1998: An assessment of satellite remotely-sensed land cover parameters in quantitatively describing the climatic effect of urbanization. *Int. J. Remote Sens.* 19, 1663–1681. <https://doi.org/10.1080/014311698215171>
- Pal, S. and Ziaul, S.K., 2017: Detection of land use and land cover change and land surface temperature in English Bazar urban center. *Egyptian J. Remote Sens. Space Scie* 20, 125–145. <https://doi.org/10.1016/j.ejrs.2016.11.003>
- Park, J., Kim, J.H. Lee, D.K., Park, C.Y., and Jeong, C.G., 2017: The influence of small green space type and structure at the street level on urban heat island mitigation. *Urban Forest. Urban Green.* 21, 203–212. <https://doi.org/10.1016/j.ufug.2016.12.005>
- Peterson, T.C., 2003: Assesment of urban versus rural in situ surface temperature in the contiguous Unites States: No difference found, *J. Climate* 18, 2941–2959. [https://doi.org/10.1175/1520-0442\(2003\)016<2941:AOUVRI>2.0.CO;2](https://doi.org/10.1175/1520-0442(2003)016<2941:AOUVRI>2.0.CO;2)
- Qin, Z., Karnieli, A., and Berliner, P., 2001: A mono-window algorithm for retrieving land surface temperature from Landsat TM data and its application to the Israel-Egypt border region. *Int. J. Remote Sens.* 22, 3719–3746. <https://doi.org/10.1080/01431160010006971>
- Ranagalage, M., Estoque, R.C., Handayani, H.H., Zhang, X., Morimoto, T., Tadono, T., and Murayama, Y., 2017: Relation between Urban Volume and Land Surface Temperature: A Comparative Study of Planned and Traditional Cities in Japan. *Sustainability* 10 (7), 2366. <https://doi.org/10.3390/su10072366>

- Rasul, A., Balzter, H., Smith, C., Remedios, J., Adamu, B., Sobrino, J.A., Srivani, M and Weng, Q., 2017: A review on remote sensing of urban heat and cool island, *Land* 6(38), 1–10. <https://doi.org/10.3390/land6020038>
- Ray, T.W., 1994: Vegetation in remote sensing FAQs, Applications, ER Mapper, Ltd., Perth, unpaginated CD-ROM. <https://doi.org/10.1155/2017/1353691>
- Rousta, I., Sarif, M. O., Gupta, R. D., Olafsson, H., Ranagalage, M., Murayama, Y., Zhang, H. and Mushore, T.D., 2018: Spatiotemporal Analysis of Land Use/Land Cover and Its Effects on Surface Urban Heat Island Using Landsat Data: A Case Study of Metropolitan City Tehran (1988–2018: *Sustainability* 10, 4433. <https://doi.org/10.3390/su10124433>
- Shahmohamadi, P., Sodoudi, S., and Cubasch, U., 2013: Mitigation of Urban Heat Island Effects as an Environmental Phenomena in Tehran. *Caspian J. Appl. Sci. Res.* 2(8), 126–135.
- Shahmohamadi, P., Chen-Ali, A.I., Abdullah, N.A.G., Maulud, K.N.A., Tahir, M.M., and Mohd-Nor, M.F.I., 2015: The Conceptual Framework on Formation of Urban Heat Island in Tehran Metropolitan, Iran: A Focus on Urbanization Factor. *Select. Topics Power Syst. Remote Sens.* 251–259. Corpus ID: 73707678
- Shamsipour, A., Mahdian Mahforouzi, M., and Akhavan, H., 2012: An Integrated Study on the Urban Heat Island Formation in Tehran. *Geophys. Res. Abstr., EGU2012-PREVIEW* 14. <https://doi.org/10.1016/j.buildenv.2010.04.001>
- Sodoudi, S., Shahmohamadi, P., Vallack, K., Cubasch, U., and Chi-Ani, A.I., 2014: Mitigating the Urban Heat Island Effect in Megacity Tehran. *Adv. Meteorol.*, Article ID 547974, 1–19. <https://doi.org/10.1155/2014/547974>
- Soltani, A. and Sharifi, E., 2017: Daily variation of urban heat island effect and its correlations to urban greenery: A case study of Adelaide. *Front. Architect. Res.* 6, 529–538. <https://doi.org/10.1016/j.foar.2017.08.001>
- Streutker, D.R., 2003: Satellite-measured growth of the urban heat island of Houston, Texas. *Remote Sens. Environ* 85, 282–289. [https://doi.org/10.1016/S0034-4257\(03\)00007-5](https://doi.org/10.1016/S0034-4257(03)00007-5)
- Sun, Q., Tan, J. and Xu, Y., 2010: An ERDAS image processing method for retrieving LST and describing urban heat evolution: A case study in the Pearl River Delta Region in South China. *Environ. Earth Sci* 59, 1047–1055. <https://doi.org/10.1007/s12665-009-0096-3>
- Van de Griend, A.A., and Owe, M., 2003: On the relationship between thermal emissivity and the normalized difference vegetation index for natural surfaces. *Int. J. Remote Sens.* 14, 1119–1131. <https://doi.org/10.1080/01431169308904400>
- Voogt, J.A. and Oke, T.R., 2003: Thermal remote sensing of urban climates. *Remote Sens. Environ.* 86, 370–38. [https://doi.org/10.1016/S0034-4257\(03\)00079-8](https://doi.org/10.1016/S0034-4257(03)00079-8)
- Weng, Q., 2001: A remote sensing-GIS evaluation of urban expansion and its impact on surface temperature in the Zhujiang Delta, China. *Int. J. Remote Sens.* 22, 1999–2014. <https://doi.org/10.1080/713860788>
- Weng, Q., 2003: Fractal analysis of satellite-detected urban heat island effect. *Photogram. Engin. Remote Sens* 69, 555–566. <https://doi.org/10.14358/PERS.69.5.555>
- Weng, Q., Lu, D., and Schubring, J., 2004: Estimation of land surface temperature–vegetation abundance relationship for urban heat island studies. *Remote Sens. Environ* 89, 467–483. <https://doi.org/10.1016/j.rse.2003.11.005>
- Weng, Q., Lu, D., and Liang, B., 2006: Urban Surface Biophysical Descriptors and Land Surface Temperature Variations. *Photogram. Engin. Remote Sens* 72, 1275–1286. <https://doi.org/10.14358/PERS.72.11.1275>
- Weng, Q., Liu, H., and Lu, D., 2007: Assessing the effects of land use and land cover patterns on thermal conditions using landscape metrics in city of Indianapolis, United States. *Urban Ecosyst.* 10, 203–219. <https://doi.org/10.1007/s11252-007-0020-0>
- Weng, Q. and Lu, D., 2008: A sub-pixel analysis of urbanization effect on land surface temperature and its interplay with impervious surface and vegetation coverage in Indianapolis, United States. *Int. J. Appl. Earth Observ. Geoinform.* 10, 68–83. <https://doi.org/10.1016/j.jag.2007.05.002>
- Xiao, R., Weng, Q., Ouyang, Z., Li, W., Schienke, E.W., and Zhang, W., 2008: Land surface temperature variation and major factors in Beijing, China. *Photogram. Engin. Remote Sens* 74, 451–461. <https://doi.org/10.14358/PERS.74.4.451>

- Xu, H., 2005: A study on information extraction of water body with the Modified Normalized Difference Water Index (MNDWI). *J. Remote Sens.* 9, 511–517. Corpus ID: 133201908
- Xu, H., 2007: Extraction of urban built-up land features from Landsat imagery using thematic-oriented index combination technique. *Photogram. Engin. Remote Sens* 73, 1381–1391.
<https://doi.org/10.14358/PERS.73.12.1381>
- Yuan, F. and Bauer, M.E., 2007: Comparison of impervious surface area and normalized difference vegetation index as indicators of surface urban heat island effects in Landsat imagery. *Remote Sens. Environ.* 106, 375–386. <https://doi.org/10.1016/j.rse.2006.09.003>
- Zha, Y., Gao, J., and Ni, S., 2003: Use of normalized difference built-up index in automatically mapping urban areas from TM imagery. *Int. J. Remote Sens.* 24, 583–594.
<https://doi.org/10.1080/01431160304987>
- Zhao, H.M. and Chen, X.L., 2005: Use of normalized difference bareness index in quickly mapping bare areas from TM/ETM+. *Geosci. Remote Sens Symp* 3(25–29), 1666–1668.
<https://doi.org/10.1109/IGARSS.2005.1526319>
- Zhang, J., Wang, Y., and Li, Y., 2006: A C++ program for retrieving land surface temperature from the data of Landsat TM/ETM+ band6. *Comput. Geosci.* 32, 1796–1805.
<https://doi.org/10.1016/j.cageo.2006.05.001>
- Zhang, J., Wang, Y., and Wang, Z., 2007: Change analysis of land surface temperature based on robust statistics in the estuarine area or Pearl River (China) from 1990 to 2000 by Landsat TM/ETM+ data. *Int. J. Remote Sens.* 28, 2383–2390. <https://doi.org/10.1080/01431160701236811>
- Zhou, D., Zhao, S., Liu, S., Zhang, L., and Zhu, C., 2014: Surface urban heat island in China's 32 major cities: Spatial patterns and drivers, *Remote Sens. Environ.* 152, 51–61.
<https://doi.org/10.1016/j.rse.2014.05.017>
- Zhou, D., Zhao, S., Zhang, L., Sun, G., and Liu Y., 2015: The footprint of urban heat island effect in China. *Sci. Rep.* 5, 11160. <https://doi.org/10.1038/srep11160>